Effect of TiO_2 blocking layer synthesised by a sol–gel method in performances of fluorine-doped tin oxide/TiO_2/dyed-TiO_2/electrolyte/pt/fluorine-doped tin oxide solar cells based on natural mallow dye

Zouhour Kadachi[1], Moufida Ben Karoui[2], Tarek Azizi[1], Rached Gharbi[1]

[1]*Laboratoire des Semi-conducteurs et Dispositifs Electroniques, Ecole Nationale Supérieure d'Ingénieurs de Tunis. University of Tunis, 05 Av. Taha Hussein 1008 Montfleury, Tunis, Tunisia*
[2]*Laboratoire de Photovoltaïque, Centre de Recherche et des Technologies de l'énergie, Technopole de Borej-Cedria, BP 95, Hammam-Lif, Tunis 2050, Tunisia*
E-mail: rached.gharbi@esstt.rnu.tn

Published in Micro & Nano Letters; Received on 2nd May 2015; Revised on 3rd December 2015; Accepted on 10th December 2015

Titanium dioxide (TiO2) thin film prepared by sol–gel technique and deposed by spin coating was used as the blocking layer between fluorine doped tin oxide and dyed TiO2 photoanode deposed by doctor blade in dye-sensitised solar cell (DSSC). The synthesised films show a polycrystalline structure at annealing temperature of 400°C with small amount of amorphous phase observed at 300°C. The values of the electrical conductivity varies from 0.11 to 1.17 Ω^{-1} cm^{-1} for one and two layers thin films, respectively, and the corresponding activation energies decreased as a function of the thickness, it passes from 109 meV for one layer to 55 meV for two layers. The photoanode of the DSSC was sensitised by the mallow diluted in ethanol having absorption spectra with two peaks, one around 480 nm (blue light) and the second at 665 nm (red light) attributable to the chlorophyll mixture. Improvement of the electrical performance is due to the increased electron lifetime and decreased of the recombination process showed by the open circuit voltage decay measurement. The lifetime values increase from 0.80 ms for the cell without blocking layer to 1.24 ms for the cell based on the blocking layer.

1. Introduction: Dye-sensitised solar cells (DSSCs) have been considered as a promising solution for harnessing solar power due to its ease of fabrication and their relative low cost compared with the conventional solar cells [1]. DSSCs consist of sensitising dye, titanium dioxide (TiO_2) porous film (anode electrode), electrolyte and the counter electrode. Under the effect of light radiation, the excited dye injects electrons into the conduction band of the TiO_2 electrode. Injected electrons are transported with diffusion toward the transparent conductive oxide (TCO) and consequently reach the counter electrode which was platinised in order to improve catalytic activity [2]. The oxidised dye accepts electrons from the electrolyte (redox mediator) regenerating the ground state and new cycle is started. The bandgap of the photoanode TiO_2 (3.2 eV) is too wide to adsorb most of the solar radiation especially the visible light [3], and the optical absorption is limited only to the ultraviolet region. Therefore, the dye used as photosensitiser should be able to harvest the sunlight and transfer it into electrical energy by absorbing the visible light. The limited availability and high cost of the transition metal compound such as ruthenium with their undesirable environmental impact [4] have led to the search for cheaper and safer dyes. There have been some interesting explorations of natural dyes for the DSSC application [5–7].

The benefits of the dye solar cells consist mainly of the low cost and the ease of fabrication. However, the charge recombination process limited the performance of the solar cell. Therefore, it is necessary that the effective lifetime of electrons in the DSSC is longer than the transit time of the electron via the photoanode of TiO_2. Many works in the literature try to inhibit the process of the recombination between the semiconductor TiO_2 which is characterised by the fast recombination of electron–hole pairs [8] and the electrolyte such as the mixing of the TiO_2 with a new material as silver, aluminium-coated TiO_2 anode [9, 10] and ZnO-coated TiO_2 electrode [11]. For the recombination occurred at fluorine-doped tin oxide (FTO)/TiO_2 interface, many works deposed a thin and uniform film between FTO substrate and mesoporous TiO_2 as a blocking layer. The literature has shown that an average improvement of 10–30% of the power conversion efficiency can be carried out using the blocking layer [12]. In this work we have synthesised a TiO_2 thin film by sol-gel spin coating technique as blocking layer between TCO and TiO_2 layer deposed by doctor blade used as the photoanode in DSSC. We have observed an improvement of the power conversion efficiency compared with the cell without blocking layer.

2. Experimental details

2.1. Preparation of the blocking layer and the photoanode: The TiO_2 thin films were synthesised using sol–gel method and deposited by spin coating [13] and used as the blocking layer of the photoanode. The sol–gel process with a simple modification was used for the synthesis of pure and dyed TiO_2 powder as the photoanode of DSSC. The white precipitate was dried at 150°C for 12 h to obtain fine particles of pure TiO_2 powder. The mixing of the natural dye during synthesis of TiO_2 results in a green brownish precipitation and this suspension was also dried at 150°C for 12 h to obtain fine particles of dye mixed TiO_2.

2.2. Fabrication of DSSC: For the fabrication of the DSSC (1.0 cm^2 active area), the obtained dyed TiO_2 powder nanoparticles was used to prepare the photoanode, it was grinded and made into a homogeneous paste. A film of TiO_2 was coated and repeated twice using doctor-blade technique on the blocking layer deposited by spin coating (Fig. 1) to form a thick layer. Then, it was sintered at a temperature of 250°C for 3 h to remove the organic benders and solidify the TiO_2 on the conductive glass substrates. Later, the photoelectrode dyed TiO_2 was immersed again for 5 h in a natural dye (mallow). The counter electrode was coated with a catalytic material for electron transfer platisol T/SP and the photoanodes were joined together. The liquid electrolyte (I^+/I_3^-, Iodolyte AN-50) was poured through the fine holes in the two electrodes carefully and sealed to prepare TiO_2-based conventional DSSC.

doi: 10.1049/mnl.2015.0154

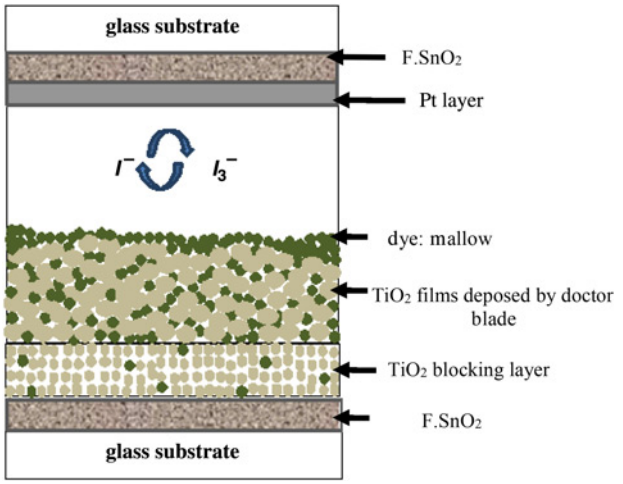

Fig. 1 *Schema of the realised DSSC with blocking layer*

2.3. Characterisation techniques: The morphology of the bottom layer thin films deposed by spin coating technique were observed using atomic force microscopy in tapping mode of a Topometrix TMX 2000. The electrical characterisation was performed using DC conductivity measurements in air and vacuum cryostat under thermal excitations (300–460 K) and the resulting current was measured by a Keithley 6517 A electrometer, while the temperature was adjusted by a 320 Auto tuning Lakeshore temperature controller.

X-ray diffraction (XRD) technique was used to identify the crystalline structure of the photoanode by an X'pert Pro X-ray diffractometer, with $\Delta 2\theta = 5$–$60°$, 0.033° as increment, integration time 50 s and Cu Kα1 radiation, $\lambda = 1.5406$ Å. To evaluate the absorbance of films, we used the UV–Vis spectrophotometer (UV-Cecil CE 3041) in the region 400–800 nm.

The current–voltage characteristics of realised DSSC were measured under AM1.5 using a density of power 100 mW/cm^2 and Keithly electrometer 6517 A at room temperature. Reading parameters were carried out by developed software using LabVIEW through the RS232 serial intelligent and operator procedures Keithly device.

The open circuit voltage decay (OCVD) technique has been employed to study the electron lifetime in DSSC devices. It has been used to explore the electron recombination process and supplies a continuous reading of the electron lifetime as a Voc curve. In OCVD measurement, the lighting was extinguished in a stable state, and then the decay of photovoltage (Voc) was monitored. A pure white LED and a microcomputer coupled to the digital oscilloscope (Tektronix) were used for the OCVD measurements.

3. Results and discussions: Thin films synthesised by the sol–gel technique and deposed by spin coating develops a crystalline phase corresponding to the titanium oxide anatase phase with a preferential orientation (101) at annealing temperature close to 400°C as given in the previous work [13]. At the heat treatment temperature below 400°C, the thin films grow in amorphous phase. The grain size of the film varied from 11.5 to 27.5 nm (Table 1) as a function of the temperature and the thickness.

The same observation and especially the anatase phase which is suitable for the solar cells application was found for the synthesised photoanode used for the solar cell. Fig. 2 gives the structural phase and crystalline size information of the powder XRD pattern of the pure, dyed TiO_2 nanoparticles powder and the thin film annealed at 250°C for 3 h obtained by modified sol–gel method and deposited by doctor blade. The intensity of the peak around 25° for the dyed TiO_2 powder is higher than for pure TiO_2, perhaps can be due to the dye which improves the crystallinity of TiO_2 as mentioned by Ananth *et al.* [6].

The XRD of the dyed film TiO_2 annealed at 250°C for 3 h shows the high intensity of the characteristic peak of the anatase phase around 25° which correspond to the (101) plan; there are another plans which confirm the anatase phase as (004), (200), (211), (204). The average particle size of the dyed TiO_2 nanoparticles in anatase phase varied from 10 to 26.58 nm.

The confirmation of the crystallisation process studied by XRD of TiO_2 films one and two layers deposited by spin coating was carried out by atomic force microscopy (AFM) observation and the experimental results are shown in Fig. 3. We notice that the increase of the annealing temperature influences on film morphology and the surface topography is composed by different particles size with irregular shapes. When the annealing temperature is increased, the well-separated nanoparticles in films get larger, starting to agglomerate and then forming clusters. This should promote the formation of large grains rougher and more crystalline layers as verified by the results of the XRD of the thin layers.

We also note that the roughness of the layers increases with the raise of the annealing temperature. This increase of the surface roughness is strongly correlated with the grain size. When the grains become increasingly large, the density of grain boundaries decreases (higher compactness), which results in a higher surface roughness values. For example, the roughness increases from 13 nm for one layer to 22 nm for two layers when the temperature of annealing passes from 400 to 600°C. These results are comparable to those determined by Calderon-Moreno *et al.* [14] who show that for 450°C the values of the roughness are between 12 and 14 nm and it increases to 20 nm for two layers.

The effect of annealing temperature and crystallisation of the films has not only an impact on structural and morphological proprieties, but also it affects the electrical parameters. The variation of electrical conductivity of the thin films one and two layers at ambient temperature is given at Table 1.

The increase of the electrical conductivity can be correlated with the grain size as given in Table 1 which depends on annealing temperature and the thickness; and it is interpreted by the improvement of the crystallinity of the layers. For example at 500°C, the crystallite size varies from 18 nm for one layer to 25 nm for two layers and the electrical conductivity increases from 0.11 Ω^{-1} cm^{-1} for one layer to 1.17 Ω^{-1} cm^{-1} for two layers. The conductivity of polycrystalline film depends on the crystallites joined at their surfaces via grain boundaries. In fact, the crystallite size decreases depending on the reduction of the layer thickness which results in the raise of the trapping states in the grain boundaries that are capable of

Table 1 Electrical conductivity, activation energy and crystallite size of TiO_2 thin films for different annealing temperatures

	σ, Ω^{-1} cm^{-1}		E_a, meV		L, nm		Mean thickness, nm	
Temp., °C	One layer	Two layers	One layer	Two layers	One layer	Two layers	One layer	Two layers
300	–	–			–	–	70.3	–
400	0.11	–	109		10.7		65.6	–
500	0.12	1.14	65	58	18.0	25.85	60.6	95.4
600	0.20	1.17	60	55	20.9	31.3	61.6	94.6

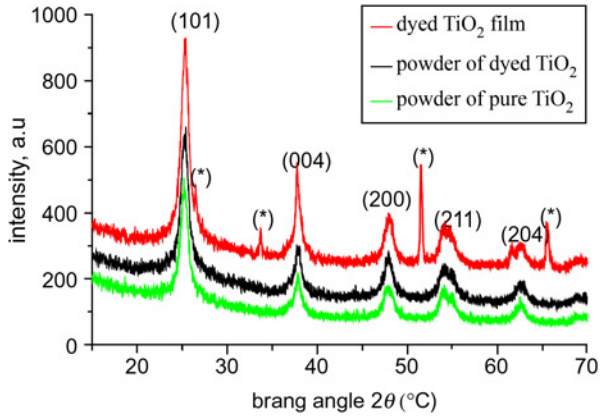

Fig. 2 *XRD spectra of pure, dyed TiO_2 powder and dyed TiO_2 film sintered at 250°C. (*): substrate F.SnO_2*

capturing the free carriers. Consequently, the growth of the grain size can lead to a reduction of the grain boundary and the improvement of the electrical conductivity. The same observation was mentioned by A. Yildiz *et al.* [15]. The activation energy is deduced from the variation of conductivity as a function of the temperature measurement and given by the following relation:

$$\sigma = \sigma_0 \times \exp\left(\frac{-E_a}{kT}\right) \tag{1}$$

E_a is the activation energy, k is the Boltzmann constant, σ_0 is a constant and T is a temperature. We report in Fig. 4 the variation of the electrical conductivity as a function of temperature and number of layers.

We report in Fig. 4 the variation of the electrical conductivity as a function of temperature and number of layers.

The Arrhenius plot provides a descendent linear curve. The exploitation of the slope gives the values of the energy activation which varied from 0.109 to 0.060 meV for one layer and from 0.058 to 0.055 meV for two layers as annealing temperature increases. The values of the activation energy of undoped TiO_2 thin layers are very small compared with that of optical gap. This implies that the TiO_2 is an n-type semiconductor means that the

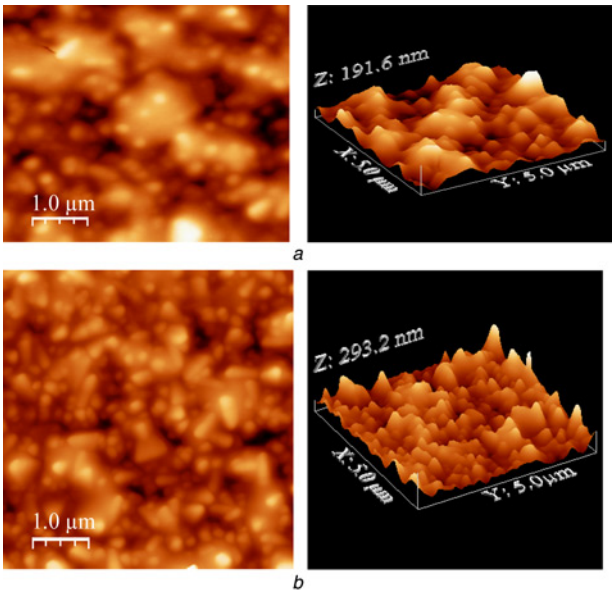

Fig. 3 *AFM surface morphology images of the TiO_2 thin films obtained after various annealing temperatures at 400°C and 600°C*
a One layer
b Two layers

Fermi level is near the minimum of the conduction band (Ec) and the concentration of the donor defects is high in the material. However, the increase of the energy activation reflecting a remoteness of Fermi level of the conduction band shows bad crystallisation of the films due to the small size of crystallites. According to the obtained values presented in Table 1, the activation energy E_a decreases with increasing temperature and thickness. This is a consequence of the reduction of the concentration of the donor defects (anion vacancies) and the increase of the crystallites size as noticed by A. Yildiz *et al.* [15].

The UV–Vis absorption spectra of pure and dyed TiO_2 films synthesised by modified sol–gel method and deposited by doctor blade are given in Fig. 5. We note that the pure TiO_2 does not absorb above 375.61 nm which corresponds to the UV region. The absorption spectra of the extracted dye mallow diluted in ethanol (Fig 5*a*) shows two peaks, one around 480 nm (blue light) and the second at 665 nm (red light) attributable to the chlorophyll mixture [6]. The absorption spectrum of the natural dyed TiO_2 in Fig. 5*b* revealed the improvement of the light photon absorption and the extension of the absorption edge which is shifted to the higher energy compared with the pure TiO_2. It shows two sharp absorption peaks at 345.80 and at 669.28 nm and a broad absorption peak at the beginning of the visible region 433.22 nm. The intensity of same peaks relating to the dyed TiO2 becomes very weak and some others are suppressed. This can be interpreted by that these types of natural dye molecules are adsorbed to the oxide surface which leads to the enhancement of the absorption. The UV cutoff wavelength (λ_{c1}) of pure TiO_2 is 375.60 nm, the bandgap was calculated by this relation $E_g(\text{eV}) = 1239.8/\lambda$ and found as 3.30 eV, however, the cutoff wavelength (λ_{c2}) of dyed TiO_2 is 420.17 nm and the bandgap was calculated as 2.95 eV. The reduce in bandgap is related to the increase of absorption wavelength which results in enhancement of photosensitisation of the TiO_2 nanoparticles as observed by S. Ananth *et al.* [6].

The photovoltaic parameters of prepared cells, as the short-circuit current density (J_{sc}, mA), the open circuit voltage (V_{oc}, mV), fill factor (FF) and efficiency ($\eta\%$) were determined from the *J–V* characteristics (Fig. 6), the fill factor FF and efficiency were calculated using the following equations:

$$\text{FF} = \frac{J_{max} V_{max}}{J_{sc} V_{OC}} \tag{2}$$

$$\eta = \frac{P_{max}}{P_{in}} = \frac{V_{max} J_{max}}{P_{in}} = \frac{\text{FF} \times (V_{OC} \times J_{sc})}{P_{in}} \tag{3}$$

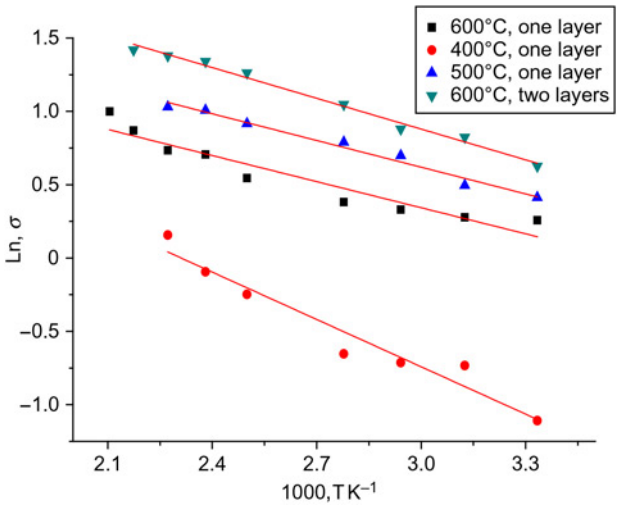

Fig. 4 *Variation of conductivity as a function of 1000/T*

doi: 10.1049/mnl.2015.0154

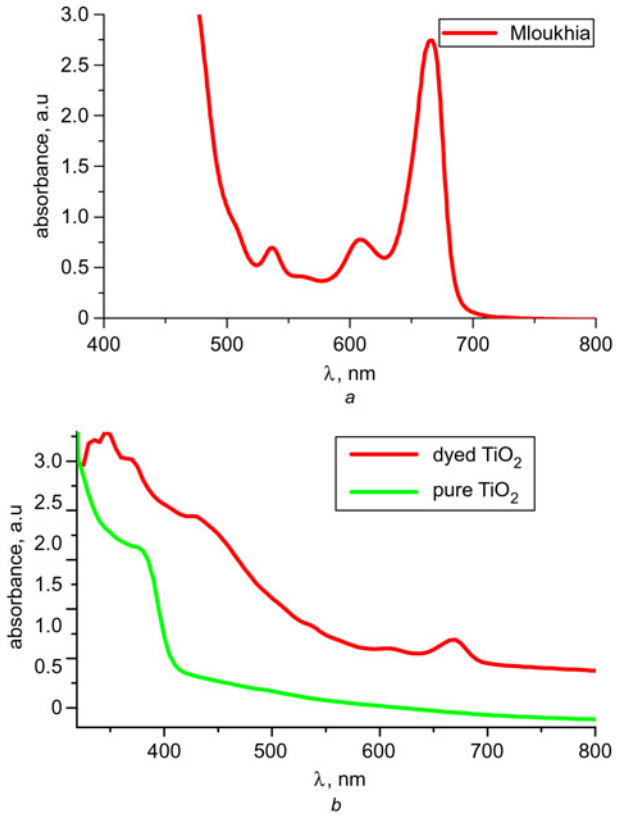

Fig. 5 *UV–Vis absorption spectra of pure and dyed TiO_2 films synthesised by modified sol–gel method*
a UV–Vis absorption spectra of mallow Mloukhia diluted in ethanol
b Absorption spectra of pure and dyed TiO_2

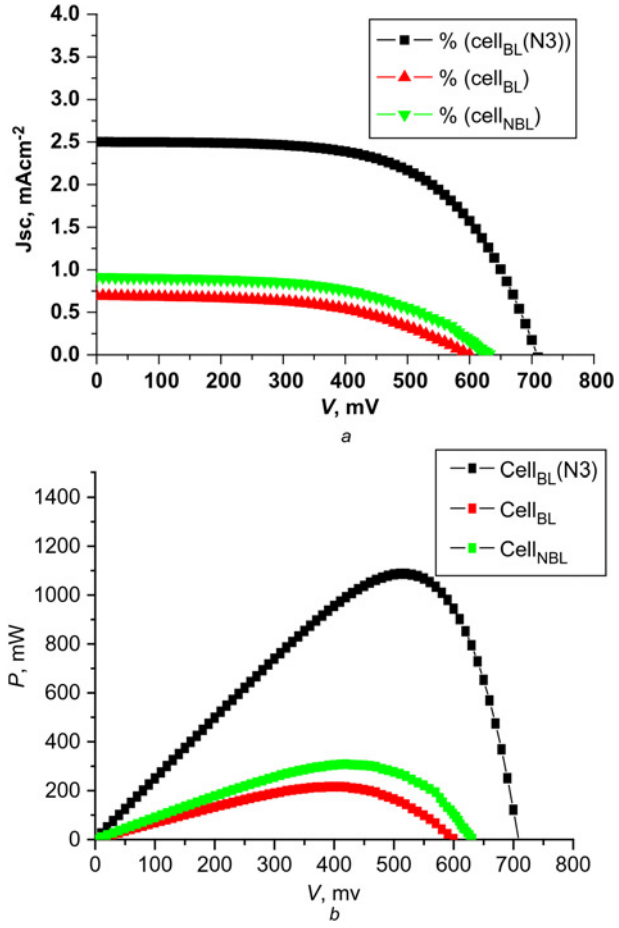

Fig. 6 *Measured current–voltage (J–V) characteristics and power–voltage characteristics of the three formed DSSCs*
a J–V characteristic curves of a dye solar cell based mallow and organic dye (N3)
b Power–voltage characteristics

In Fig. 6*a*, we give the measured current–voltage (*J–V*) characteristics of the three formed DSSCs, while the power–voltage characteristics were given in Fig. 6*b*.

The current–voltage curves of DSSC using mallow as dye has a typical behaviour of a solar cell. The maximum power point is determined from the *P–V* curves (Fig. 6*b*) which show a maximum correspond to the J_{max}. The realised solar cell based on the natural dye (mallow) and with the blocking layer ($cell_{BL}$) admitted efficiency equal to 0.32% with a fill factor of 54.24% and an open-circuit voltage of 0.63 V as shown in the *J–V* characteristics. However, The N3-Dye based DSSC with the blocking layer device exhibits $J_{sc} = 2.5$ mA/cm^{-2}, $V_{OC} = 700.06$ mV and a fill factor equal to 62.38% resulting in an overall efficiency of 1.14%. These results reveal that using N3 dye in DSSC shows significant increment in fill factor and conversion efficiency. We can observe (Fig. 6*a*) a decrease in series resistance which reflects the improvement of *J–V* characteristics compared with the two other cells.

The efficiency of the cell sensitised with the natural dye (mallow) is enhanced compared with the cell without blocking layer ($Cell_{NBL}$) obtained by A. Torchani *et al.* [16].

This improvement of the conversion efficiency is due in particular to two main reasons: the first one is the effect of direct mixing of natural dye during the synthesis of the photoanode by modified sol–gel technique which contributes to obtain more dye adsorption and less dye aggregation. The second one is the use of this synthesis method in the deposition of a TiO_2 blocking layer with a smaller particle size which was baled more efficiently on the surface of the FTO substrate. This minimises the size of the voids between the particles, which reduces the percolation of the electrolyte on the FTO glass and therefore the increase of the J_{sc}. On the other hand, improvement of the interfacial contact between FTO substrate and mesoporous TiO_2 layer through the blocking layer affects the efficiency enhancement.

In addition, the blocking layer has a bandgap and an optical absorption coefficient much higher than the TiO_2 layer of the photoanode which leads to a more sunlight passes to the photoanode and producing more photo-excited electrons. Moreover, it creates an energy barrier that can prevent the injected electrons from the dye to recombine back to dye molecules or electrolyte species. It is possible by using a modified sol–gel method for the synthesis of the dyed TiO_2 photoanode to enhance the dye loading and reducing his aggregation.

The lack of available bonds between the dye and TiO_2 molecules which electrons can transport from the excited dye molecules to the TiO_2 film can be improved more by the great purification of the dye and extraction of the molecule responsible for the photo-generation of electrons in the semiconductor conduction band. The improvement of the performance of the DSSC is verified by the OCVD measurements. In fact, the electronic process of electrons recombination at the interfaces of FTO/electrolyte/TiO_2 can be described by the charge carrier lifetime and deduced from the derivative of the V_{OC} decay curve after turn off the light using the equation

$$\tau = -\frac{k \times T}{q} \times \left[\frac{dV_{OC}}{dt}\right]^{-1} \quad (4)$$

Where k is the Boltzmann's constant, q is the elementary charge and T is the temperature.

Fig. 7*a* shows the variation of voltage decay curves open circuit as a function of the time for the $cell_{BL}$ and the $cell_{NBL}$ after the light

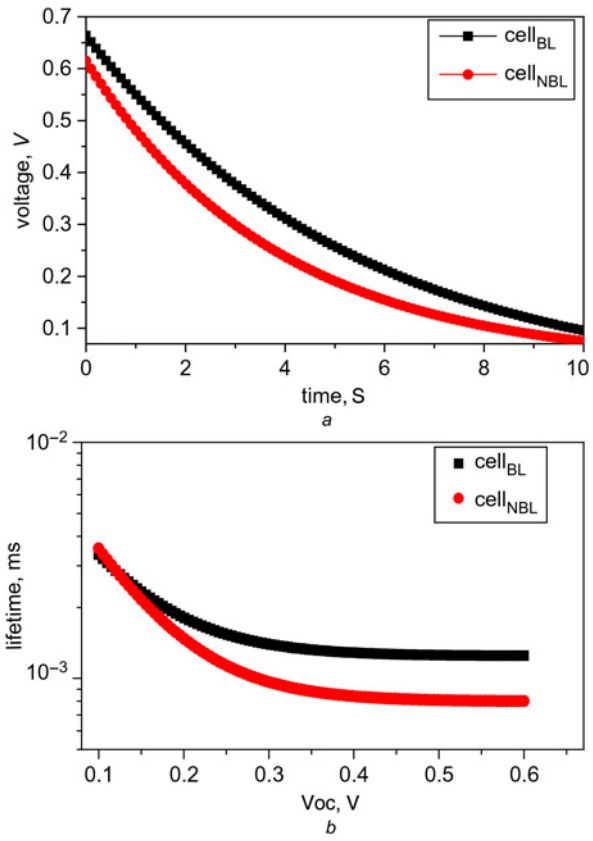

Fig. 7 *Variation of voltage decay curves open circuit as a function of the time for the cell$_{BL}$ and the cell$_{NBL}$ after the light was extinguished*
a OCVD curves of the two cells sensitised by natural dye
b Calculated electron life time as function of open-circuit voltage of the two cells

was extinguished. The decay of the voltage shows the decrease of the electron concentration in the conduction band of TiO_2 which is mainly caused by the charge recombination occurred at FTO/electrolyte and TiO_2/electrolyte interfaces. As the source of the illumination is cutoff, the photo-generation was stoped and the voltage decay rapidly falls off to 0 V as a result of uninterrupted charge recombination. It is clear that the cell$_{BL}$ exhibit a slower decay than the cell$_{NBL}$ indicating that the presence of the blocking layer can inhibit the recombination of the charge carriers.

The electron lifetime is then obtained by analysing the time (t) dependent of V_{OC} decay and it was calculated as a function of voltage V_{OC} for the two cells as shown in Fig. 7*b*. From the above measurements, an improvement of the charge lifetime was evidenced for the cell$_{BL}$, and it is clear that the electron lifetime of this cell is longer than the cell$_{NBL}$. The lifetime values at 0.6 V of the two cells were found to be 1.24 and 0.80 ms for cell$_{BL}$ and cell$_{NBL}$, respectively, which is in accordance with the cell's performance.

4. Conclusion: We have prepared nanocrystalline TiO_2 thin films by employing a simple and inexpensive sol–gel spin coating technique. The realised thin film in two layers was used as the blocking layer between FTO substrate and TiO_2 layer deposited by doctor blade in the DSSC. Annealing has been found to have a strong influence on structural, surface morphology, optical and electrical properties of nanocrystalline TiO_2 thin films. From the study of the electrical properties, we have found that the transport mechanism of charge carriers is strongly influenced by crystallite size and the thickness of the films.

The modified sol–gel method for the synthesis of the dyed TiO_2 photoanode has shown an improvement of 10% in efficiency, characterised by the more adsorption of the dye and less dye aggregation. The direct mixing of natural dye is a promising process for the uniform adsorption of dye to light and therefore the efficiency of electron conversion was enhanced. In addition, the use of the blocking layer improves the performances of the DSSC through the reduction of the electron recombination which is confirmed by the calculated electron lifetime.

5 References

[1] Regan B.O., Gratzel M.: 'A low-cost, high-efficiency solar cell based on dye-sensitized colloidal TiO_2 films', *Nature*, 1991, **353**, pp. 737–740

[2] Lamberti A., Sacco A., Bianco S., *ET AL.*: 'Enhancement of electron lifetime in dye-sensitized solar cells using anodically grown TiO_2 nanotubes/ nanoparticle composite photoanodes', *Microelectron. Eng.*, 2013, **111**, pp. 137–142

[3] Song X., Yang F., Fang Q., *ET AL.*: 'Capsule-like CdS-modified TiO_2 nanocomposites with enhanced photodegradation under visible light irradiation', *Micro Nano Lett.*, 2015, **10**, pp. 157–160

[4] Hamadanian M., Safaei-Ghomi J., Hosseinpour M., *ET AL.*: 'Uses of new natural dye photosensitizers in fabrication of high potential dye-sensitized solar cells (DSSCS)', *Mater. Sci. Semicond. Process.*, 2014, **27**, pp. 733–739

[5] Ludin A., Al-Alwani M., AbuBakar M., *ET AL.*: 'Review on the development of natural dye photosensitizer for dye-sensitized solar cells', *Renew. Sustain. Energy Rev.*, 2014, **31**, pp. 386–396

[6] Ananth S., Arumanayagam T., Vivek P., *ET AL.*: 'Direct synthesis of natural dye mixed titanium dioxide nano particles by sol–gel method for dye sensitized solar cell applications', *Optik*, 2014, **125**, pp. 495–498

[7] Torchani A., Gharbi R., Fathallah M.: 'Study of natural dyes for sensitized solar cells applications', *Sens. Transducers*, 2014, **27**, pp. 185–189

[8] Deng Q., Han Y., Liu Y., *ET AL.*: 'Preparation and characterization of carbon-modified TiO_2 composite', *Micro Nano Lett.*, 2014, **09**, pp. 471–474

[9] Peng W., Zeng Y., Gong H., *ET AL.*: 'Silver –coated TiO_2 electrodes for high performance dye-sensitized solar cells', *Solid State Electron.*, 2013, **89**, pp. 116–119

[10] Liou Y.-J., Chen Y.-J., Chen B.-R., *ET AL.*: 'XPS study of aluminum coating on TiO_2 anode of dye-sensitized solar cells', *Surf. Coat. Technol.*, 2013, **231**, pp. 535–538

[11] Chou C.-S., Chou F.-C., Ding Y.-G., *ET AL.*: 'The effect of Zno-coating on the performance of a dye-sensitized solar cell', *Sol. Energy*, 2012, **86**, pp. 1435–1442

[12] Gu Z.Y., Gao X.-D., Jiang X.M., *ET AL.*: 'Nanoporous TiO_2 aerogel blocking layer with enhanced efficiency for dye-sensitized solar cells', *J. Alloys Compd*, 2014, **590**, pp. 33–40

[13] Ben Karoui M., Kaddachi Z., Gharbi R.: 'Optical properties of nano-structured TiO_2 thin films'. *J. Phys., Conf. Ser.*, 2015, doi: 10.1088/1742–6596/596/1/012012 p. 596

[14] Calderon-Moreno J.M., Preda S., Predoana L., *ET AL.*: 'Effect of polyethylene glycol on porous transparent TiO_2 films prepared by sol–gel method', *Ceram. Int.*, 2014, **40**, pp. 2209–2220

[15] Yildiz A., Serinb N., Kasapc M., *ET AL.*: 'The thickness effect on the electrical conduction mechanism in titanium oxide thin films', *J. Alloys Compd.*, 2010, **493**, pp. 227–232

[16] Torchani A., Saadaoui S., Gharbi R., *ET AL.*: 'Sensitized solar cells based on natural dyes', *Curr. Appl. Phys.*, 2015, **15**, pp. 307–311

doi: 10.1049/mnl.2015.0154